Seventh International Conference on Computational Fluid Dynamics (ICCFD7), Big Island, Hawaii, July 9-13, 2012

ICCFD7-3902

Numerical simulation of the vortex dynamics and of the flow control around a simplified ground vehicle

Charles-Henri Bruneau (1), Emmanuel Creusé (2), Patrick Gilliéron (3)
and Iraj Mortazavi (1)
(1) Univ. Bordeaux, IMB. CNRS, UMR 5251. INRIA Bordeaux, Team MC2.
F-33400 Talence, France.
(2) Université Lille 1, LPP. CNRS, UMR 8524. INRIA Lille, Team SIMPAF.
F-59655 Villeneuve d'Ascq, France.
(3) Independent researcher
F-78640 Neauphle Le Château, France.

Abstract: The aim of this work is to better understand the impact of the vortical structures motion to the drag coefficient of a simplified ground vehicle. A theoretical study and numerical experiments show the strong relationship between the distance of the vortices to the back wall and the pressure forces. So a way to control the flow is to change the trajectories of the vortices to accelerate their removal from the wall. Numerical results show that this strategy is indeed very efficient.

Keywords: Vortex dynamics, Computational Fluid Dynamics, Square-back Ahmed body.

1 Introduction

In this work, direct numerical simulations of the two-dimensional flow around the square back Ahmed body [2], corresponding to simplified mono space cars or trucks, are considered. The incompressible Navier-Stokes system is solved in a computational domain including the square back Ahmed body on top of a road. First of all, some theoretical results on ideal convective vortex motions are analyzed to explore the best kinematics necessary to decrease the pressure force on the wall. Then, the evolution of a toy vortex added in a background stationary flow is carefully studied without or with an active control by a steady jet. This study permits to better understand the effect of the control procedure on the kinematics of one vortex and the resulting pressure force. Finally the vortex shedding of the real flow computed around the body is analyzed as we study the mean trajectory of the top and bottom vortices at the back. The effects of a closed-loop active control using blowing jets and of a passive control using porous layers [6, 7, 12] are carefully compared to the analytical model. It appears that the control can improve significantly the trajectories and the removal speeds of some vortices to reach almost the ideal motion. Consequently the pressure force is reduced and finally the drag coefficient is decreased.

2 Study and control of a single vortex

With non-viscous hypothesis, the two-dimensional vortex model is based on two theories: the circular vortex theory [10, 11] and the mirror image vortex theory [9]. The first one considers the vortex as a disk. The velocity is infinite in the center and decreases when the radius increases. To avoid the infinite velocities on the wall, the vortex position is considered to be at least as far as a classical viscous radius value ϵ from the body. The second theory allows to model the vortex sliding actions to the wall. In fact, the sliding force at the wall is the amount of the forces generated by the studied vortex and its wall mirror image vortex. Let us recall here the basis of such an approach and its extension to the force evaluation on the wall.

Let H be the height of the back wall of the vehicle characterized in its two dimensional representation by the coordinates set $x = 0$ and $-H/2 \leq z \leq H/2$, let us consider $M(0, z)$ a point on the back wall and a vortex whose center is located at point $P(x_1, z_1)$, $x_1 > 0$. If the vortex is moving, the instantaneous pressure force $F_p(t)$ induced by the vortex on the wall at time t can be evaluated by:

$$F_p(t) = \frac{\rho}{2}\frac{\Gamma^2}{\pi^2}\int_{-\frac{H}{2}}^{+\frac{H}{2}} \frac{x_1^2(t)}{(x_1^2(t) + (z - z_1(t))^2)^2} dz \tag{1}$$

where ρ is the density and Γ is the circulation of the vortex. This pressure force depends of course strongly on the circulation Γ but also on the distance of the vortex. So, a way to reduce this force is to push away the vortex.
To validate this study a numerical simulation is performed solving the 2D Navier-Stokes equations. The simulation is performed in the computational domain $\Omega = (0, 15H) \times (0, 5H)$ with a square-back Ahmed body located at the distance 5.3 from the entrance section and 0.6 from the road (Figure 1) and whose length is $L = 3.625$, by solving the penalized Navier-Stokes equations in velocity and pressure (U, p) (see [1, 5]):

$$\partial_t U + (U \cdot \nabla)U - \frac{1}{Re}\Delta U + \frac{U}{K} + \nabla p = 0 \quad in\ \Omega_T = \Omega \times (0, T), \tag{2}$$

$$div\, U = 0 \quad in\ \Omega_T, \tag{3}$$

where $K = \frac{k\Phi\overline{U}}{\nu H}$ is the non dimensional coefficient of permeability of the medium, $\overline{U}$ is the mean velocity, k is the intrinsic permeability, ν is the kinematic viscosity and Φ is the porosity of the fluid, $Re = \frac{\overline{U}H}{\nu}$ is the Reynolds number based on the height of the body. To recover the genuine Navier-Stokes equations we set

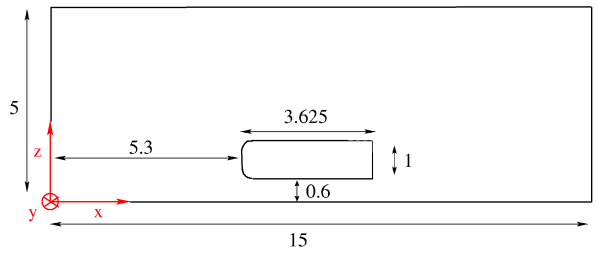

Figure 1: Computational domain around the square back Ahmed body.

$K = 10^{16}$ in the fluid. On the contrary $K = 10^{-8}$ in the solid body to get a velocity field of the same order in the solid mimicking a porous body with very low permeability. A constant Dirichlet condition is imposed upstream and on the road $\overline{U} = (\overline{u}_x, \overline{u}_z) = (1, 0)$ (corresponding to the speed of the ground vehicle) and a non reflecting boundary condition on the open frontiers (top and downstream) [4] is used.
The system of equations (2),(3) is solved by a strongly coupled approach for the physical unknowns (U, p). The time discretization is achieved using a second-order Gear scheme with explicit treatment of the convection term. All the linear terms are treated implicitly and discretized via a second-order centered finite differences scheme. The CFL condition related to the convection term requires a time step of the order of magnitude of the space step as $\overline{U} = (1, 0)$, which is relevant to have a good accuracy of the evolution of the flow and does not induce too much cpu time. A third-order finite differences upwind scheme is used for the discretization of the convection terms [8]. The efficiency of the resolution is obtained by a multigrid procedure using V cycles and a cell-by-cell relaxation smoother. A set of grids is defined starting from the 15×5 coarse mesh to the finest mesh and the number of grids is determined to get accurate results.

Here, the numerical test involves a vortex behind the back wall moving both from the bottom to the top along the wall and forward. To control the effect of this vortex on the wall, a constant blowing jet is located at two thirds of the height. When the vortex arrives in front of the jet it is pushed away as can be seen in the Figures 2 and 3. The vortex is further and there is no opposite sign vorticity along the wall. Consequently

the pressure force decreases (Figure 4). It is remarquable to see that the uncontrolled and the controlled cases for the theoretical computation of the pressure forces F_p (eq (1)) and for the numerical computation of the forces F_{p-comp} using the simulated pressure values on the wall have the same evolutions.

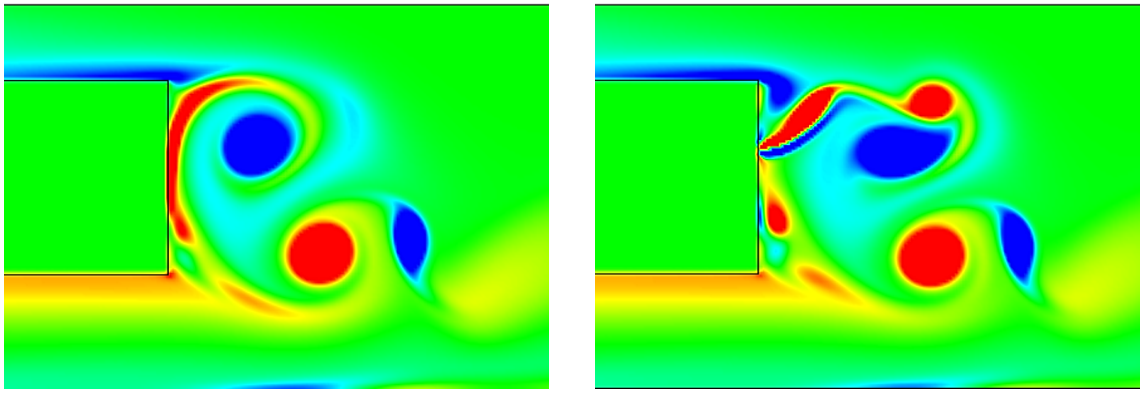

(a) uncontrolled case (b) controlled case

Figure 2: Comparison of the vorticity field in the wake of Ahmed body between the uncontrolled and the controlled cases at simulation time $t = 12$.

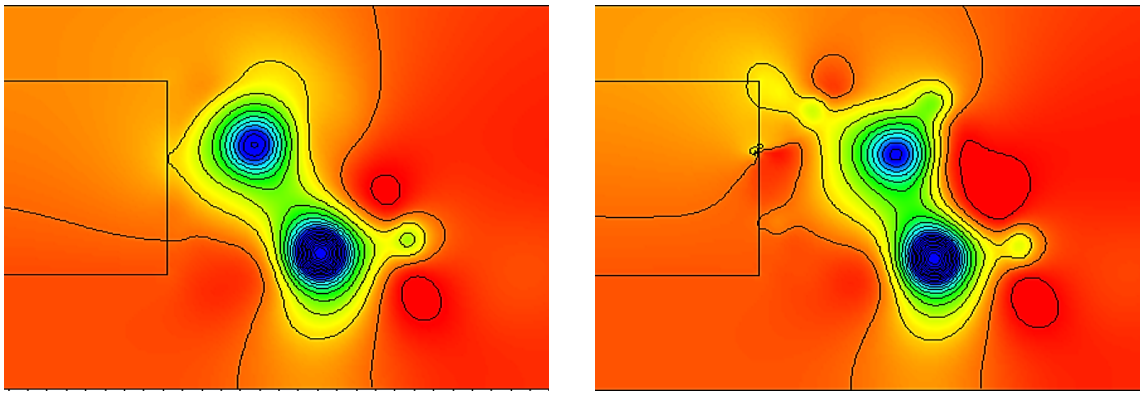

(a) uncontrolled case (b) controlled case

Figure 3: Comparison of the pressure field in the wake of Ahmed body between the uncontrolled and the controlled cases at simulation time $t = 12$.

3 Active control of the flow around a simplified ground vehicle

To remove the vortices from the back wall, an active control with blowing jets is used. The first choice is to take a constant jet of velocity $U_j = 0.6\overline{U}$ which corresponds to the forcing intensity 8×10^{-3} defined by $C_\mu = \frac{h_j}{H}\left(\frac{U_j}{\overline{U}}\right)^2$ where h_j is the size of the jet [7]. But, as the effect of the vortices is strongly linked to the pressure at the wall, an efficient choice for such a control is a closed-loop active control with the velocity of the blowing jets U_j given by:

$$U_j = \frac{U_{jmax}}{2}(1 - \beta(p_{sensors} - \bar{p}_{sensors})), \tag{4}$$

where U_{jmax} is the maximum blowing velocity (here $U_{jmax} = 1.2\overline{U}$ to get the same mean velocity than for the constant jet), β a normalized coefficient defined in such a way that $0 \leq U_j \leq U_{jmax}$ (here $\beta = 1.5$),

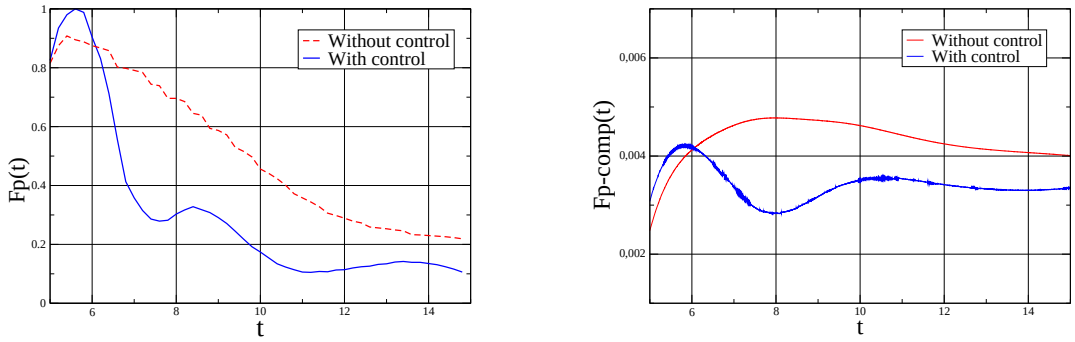

Figure 4: History of the theoretical pressure force F_p and of the pressure force computed from the numerical simulation at the back F_{p-comp} induced by the new vortex between simulation times $t = 5$ and $t = 15$.

$p_{sensors} = min(p_{sensor1}, p_{sensor2})$ the lowest pressure measured by the sensors and $\bar{p}_{sensors}$ the averaged pressure of both sensors [7], where the sensors location is shown in the Figure 5. The closed-loop active

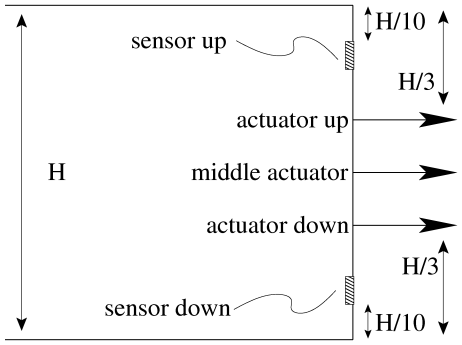

Figure 5: Location of the actuators and sensors at the back wall of the square back Ahmed body.

control techniques used in this work are composed of a jet blowing from one of the three positions of the back wall (see Figure 5).

The first study consists in comparing the instantaneous vorticity fields of the reference (uncontrolled) case to the controlled case with one actuator in the middle of the back wall. This position is chosen in order to take into account the shedding that generates both up and down vortices. Two simulations are initialized with the same reference flow in order to observe the evolution of up and down vortical structures. The first case is without control and the second is with control corresponding to a blowing closed-loop actuator which better includes the shedding frequencies of the real flow. The Figure 6 shows the time evolution and the averaged values of the drag coefficients for both cases. After two periods of shedding, the drag coefficient is considerably reduced (-20%) by the blowing control.

The Figures 7 and 8 represent the instantaneous vorticity fields for eight successive moments. The control becomes effective after $t = 3.0$ and up to this time the fields are almost identical. Then, the vortices are pushed away more quickly in the controlled case as it can be seen at simulation time $t = 5.0$ for a top vortex and at time $t = 6.0$ for a bottom vortex. To better analyze the efficiency of the control, in the Figure 9 the trajectories of two top and bottom vortices with the same initial position are compared for the uncontrolled and controlled cases. The letters $A - H$ and $a - h$ correspond to the same times in the trajectories for both simulations (see Table 1). As the Figure shows, the blowing jet pushes away very quickly the vortical structures from the back wall whereas in the uncontrolled simulation these vortices move away slowly in the

near wake of the wall. This effect is more effective on the bottom vortex as it is amplified by the jet under the body.

In order to get a quantitative estimation of the relationship between the vortex kinematics and the drag

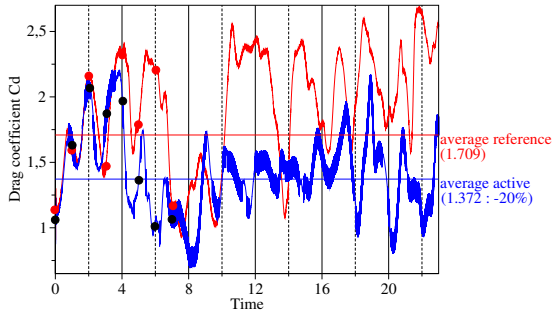

Figure 6: Evolution and mean value of the drag coefficients for the reference case and the controlled case with a closed-loop active control at the middle of the wall.

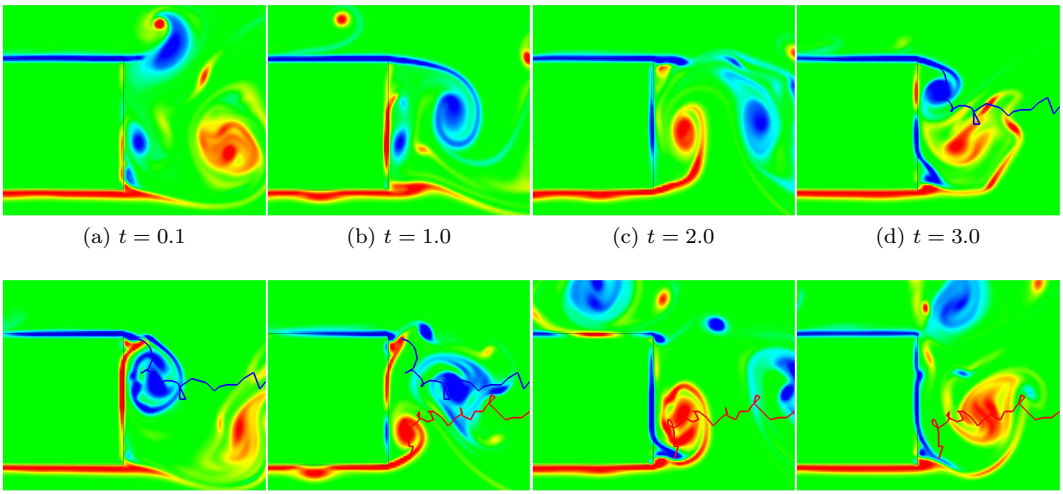

(a) $t = 0.1$ (b) $t = 1.0$ (c) $t = 2.0$ (d) $t = 3.0$

(e) $t = 4.0$ (f) $t = 5.0$ (g) $t = 6.0$ (h) $t = 7.0$

Figure 7: Vorticity fields along time for the reference case without control.

Points	A	B	C	D	E	F	G	H
Time t	2.5	3.0	3.5	4.0	4.5	5.0	5.5	6.0
Points	a	b	c	d	e	f	g	h
Time t	5.0	5.5	6.0	6.5	7.0	7.5	8.0	8.5

Table 1: Time-letters correspondences for the instantaneous vortex motion study.

reduction due to the control, an averaged estimation of several vortex motions is necessary. So the mean trajectories of the top and bottom vortices are studied for uncontrolled and controlled cases. The averaging procedure is performed for ten successive vortices on both sides of the wall from simulation time $t = 3$ until time $t = 23$. In the Figure 10 the mean uncontrolled trajectories are compared to the mean controlled ones with a closed-loop actuator at the middle of the back wall. The time-letters correspondences are given in

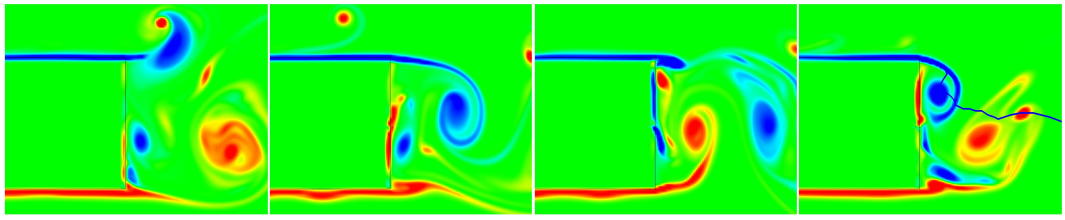

(a) $t = 0.1$ (b) $t = 1.0$ (c) $t = 2.0$ (d) $t = 3.0$

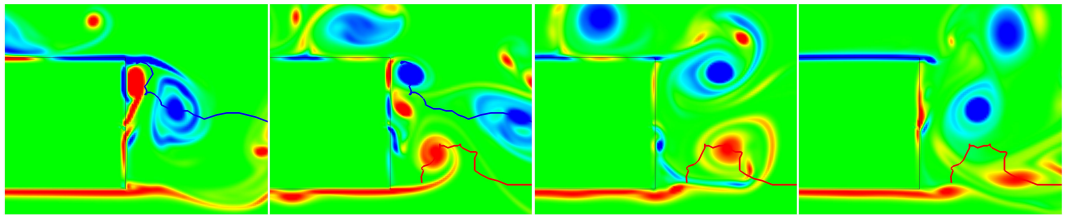

(e) $t = 4.0$ (f) $t = 5.0$ (g) $t = 6.0$ (h) $t = 7.0$

Figure 8: Vorticity fields along time for the controlled case with a closed-loop active control at the middle of the wall.

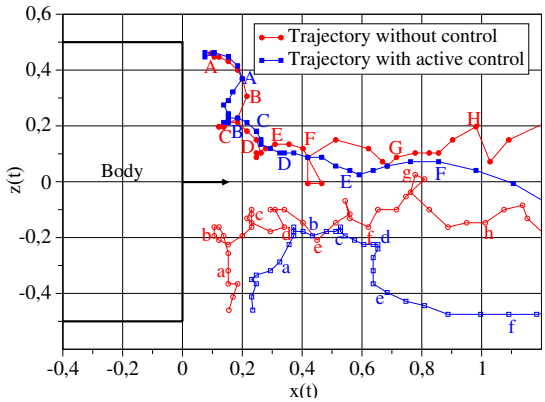

Figure 9: Comparison of trajectories for the top and bottom vortices without control and with a closed-loop active control at the middle of the wall.

Table 2, time $t = 0$ corresponds to the first time a vortex is identified by Weiss criterion [3] in the vicinity of one corner. This statistical study reveals that the control has less effect on the top vortices removal as they are naturally driven away by the flow. However, the trajectories of the bottom vortices are drastically modified as in the reference flow, the bottom vortices are pushed upwards by the flow underneath the body. In that case, like for the toy vortex study, the vortices are expelled from the body very quickly with the control.

Points	A	B	C	D	E	F	G	H
Time t	0.5	1.0	1.5	2.0	2.5	3.0	3.5	4.0

Table 2: Time-letters correspondences for the averaged vortex motion study.

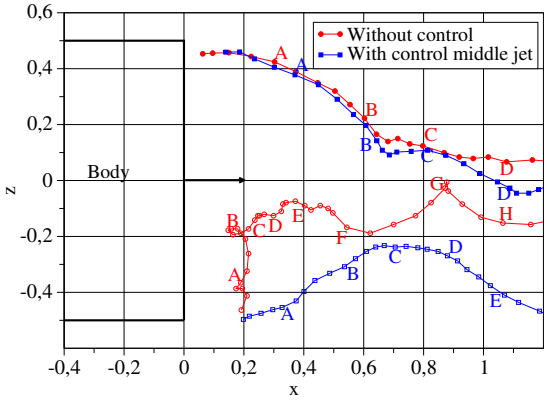

Figure 10: Comparison of averaged trajectories for the cases without control and with a closed-loop active control at the middle of the wall.

4 Conclusions

In the first part of this paper, it is emphasized that the pressure force on the back wall depends directly on the circulation and the speed of removal of the vortices. The larger this speed is, the more the pressure forces decrease and so the drag coefficient. This is confirmed by numerical simulations using a toy vortex. Then a closed-loop active control is used to reduce the drag coefficient of the square back Ahmed body. It is confirmed that such an active control is efficient for some vortices according to their trajectory. It is the case for the shedded vortices coming from the bottom edge of the back wall due to the presence of the road but there is no noticeable improvement for the vortices coming from the top edge.

References

[1] Angot, P., Bruneau, C.-H. & Fabrie, P., A penalization method to take into account obstacles in incompressible viscous flows, *Numerische Mathematik* **81**, 497-520, 1999.

[2] Ahmed, S. R., Ramm, G. & Faltin, G., Some Salient Features of the Time -Averaged Ground Vehicle Wake, *SAE-Paper* **840300**, 1984.

[3] Basdevant, C., On the validity of the Weiss criterion in two-dimensional turbulence, *Physica D* **73** n° 1-2, 1994.

[4] Bruneau, C.-H. & Fabrie, P., Effective downstream boundary conditions for incompressible Navier-Stokes equations, *Int. J. Num. Meth. Fluids* **19**, 693-705, 1994.

[5] Bruneau, C.-H. & Mortazavi, I., Passive control of the flow around a square cylinder using porous media, *Int. J. Num. Meth. Fluids* **46**, 415-433, 2004.

[6] Bruneau, C.-H., Mortazavi, I. & Gilliéron, P., Passive control around the two-dimensional square back Ahmed body using porous devices, *J. Fluids Eng.* **130**, 1-33, 2008.

[7] Bruneau, C.-H., Creusé, E., Depeyras, D., Mortazavi, I. & Gilliéron, P., Coupling passive and active techniques to control the flow past the square back Ahmed body, *Comp. & Fluids*, **38**, n° 10, 2010.

[8] Bruneau, C.-H. & Saad, M., The 2D lid-driven cavity problem revisited, *Comp. & Fluids* **35**, 326-348, 2006.

[9] Lamb, H., Hydrodynamics, *Cambridge University Press*, 1916.

[10] Milne-Thomson, L.M., Theoretical aerodynamic, *Dover*, 1966.

[11] Milne-Thomson, L.M., Theoretical hydrodynamic, *Dover*, 1968.

[12] Rouméas, M., Contribution à l'analyse et au contrôle des sillages de corps épais par aspiration ou soufflage continu, *PhD Thesis*, 2006.